Quantum-Chemical Calculations of Carbon-Isotope Fractionation in CO_2(g), Aqueous Carbonate Species, and Carbonate Minerals

James R. Rustad,*,† Sierra L. Nelmes,† Virgil E. Jackson,‡ and David A. Dixon*,‡

Department of Geology, University of California, Davis, One Shields Avenue, Davis, California 95616 and Department of Chemistry, Shelby Hall, The University of Alabama, Tuscaloosa, Alabama 35487-0336

Received: July 31, 2007; In Final Form: October 1, 2007

Quantum chemical calculations on large supermolecular carbonate−water and carbonate mineral clusters are used to predict equilibrium constants for ^{13,12}C-isotope-exchange reactions between CO_2(g), aqueous carbonate species, and the common carbonate minerals. For the aqueous species, we evaluate the influence of the size and conformational variability of the solvation shell, the exchange−correlation functional, and the basis set. The choice of exchange−correlation functional (PBE vs B3LYP), the basis set (6-31G* vs aug-cc-pVDZ), and solvation shell size (first shell only vs first shell and a partial second shell) each produce changes of ∼5−10 per mil in the reduced partition function ratio. Conformational variability gives rise to a standard error of ∼0.5 per mil using ∼10 solute−solvent conformations. The best results are obtained with the B3LYP/aug-cc-pVDZ combination, but because the improvements in the basis set and exchange correlation functional drive the reduced partition function ratios in opposite directions, reasonably good results are also obtained with the PBE/6-31G* combination. To construct molecular clusters representative of mineral environments, a new method is introduced on the basis of conservation of Pauling bond strength. Using these clusters as models for minerals, calculations of mineral−gas and mineral−aqueous carbon-isotope fractionation factors, are in good agreement with experimental measurements. Carbon-isotope fractionation factors for gas, aqueous, and mineral phases are thus integrated into a single theoretical/computational framework.

I. Introduction

^{12,13}C isotopic fractionation between gaseous CO_2(g), the aqueous carbonate species [CO_2(aq), HCO_3^-(aq), CO_3^{2-}(aq)], and the common carbonate minerals (calcite, dolomite, and aragonite) is fundamental to a variety of geochemical processes involving the carbon cycle. Several studies have reported measurements of carbon-isotope fractionation among species in the aqueous CO_2 system.[1−6] It is well-established that, at equilibrium, CO_2(aq) is isotopically lighter than CO_2(g) by about 1 part per thousand (per mil) and that the dissolved ionic species HCO_3^-(aq) and CO_3^{2-}(aq) are both isotopically heavier than CO_2(g). Historically, there has been some disagreement about the extent of fractionation of the aqueous ionic species relative to the gas,[7] but recent consensus has gathered around the work of Zhang et al.,[4] where it was found that HCO_3^-(aq) is enriched in ^{13}C by 7.9 per mil and that CO_3^-(aq) is enriched in ^{13}C by 5.9 per mil relative to CO_2(g) at 25 °C. A potential source of error results from incomplete knowledge of the speciation of HCO_3^-(aq), CO_3^{2-}(aq), and CO_2(aq). In particular, the role of ion pairs, such as $NaCO_3^-$(aq) and $NaHCO_3$(aq), on fractionating ^{12,13}C among the carbonate and bicarbonate species in solution is not well understood.[6−8] For carbonate minerals, measurements have shown that calcite is enriched by approximately 1 per mil in ^{13}C with respect to HCO_3^-(aq) and that aragonite is enriched by about 1.8 per mil in ^{13}C with respect to calcite[9,10] at 25 °C.

The difficulties of making accurate isotopic measurements on aqueous systems with dynamic chemical speciation such as carbonate and borate provide motivation for using computational chemistry approaches to help interpret experimental measurements.[11] Previous work on the aqueous boric acid/borate system[12,13] indicated that computationally affordable theoretical methods such as density functional theory (DFT) or Hartree−Fock molecular orbital (HF−MO) theory with modest double-ζ basis sets could provide fractionation factors within 1 per mil of experiment. Calculations on solute−water clusters quenched from density functional theory molecular-dynamics simulations (DFT-MD)[14] supported this conclusion. Because the calculations in refs 12 and 14 employed different basis sets, different computational approaches (HF-MO vs DFT), and different molecular cluster preparation techniques, the level of agreement between the two approaches is compelling, and suggests that per mil accuracies might be obtainable in aqueous systems without invoking computationally expensive large basis sets and/or anharmonic corrections. In mineral systems, previous work[15] using DFT pseudopotential/planewave methods in a lattice dynamics context has been able to reproduce measured fractionation between calcite and aragonite with high accuracy. Isotope fractionation factors have been measured and calculated in the gas phase to understand strong hydrogen bonds.[16]

The broad geochemical significance of the carbon cycle, controlled, in part, by aqueous carbonate species and carbonate minerals, underscores the importance of assessing the performance of theoretical methods for predicting carbon-isotope fractionation in the aqueous carbonate system. This paper reports results of a DFT and MO theory investigation of carbon-isotope fractionation between CO_2(g), aqueous carbonate species, and the major carbonate minerals (calcite, aragonite, and dolomite). The main question addressed is whether computational quantum chemical methods are capable of predicting isotopic fractionation

† University of California-Davis. E-mail for J.R.R.: rustad@geology.davis.edu.

‡ The University of Alabama. E-mail for D.A.D.: dadixon@bama.ua.edu.

10.1021/jp076103m CCC: $40.75
Published on Web 01/01/2008

factors across the range of gas, aqueous, and solid-state systems with approximately 1 per mil accuracy, close to the level needed for the calculations to be useful to the geochemical community. Two innovations introduced in this paper make it possible to address this question. First, we use DFT-MD as a systematic procedure for the generation of large numbers of solute−solvent conformations. Such an approach has been used to develop a model for aqueous Cl^- at high temperatures.[17] These methods follow on the initial work of Stillinger and Weber on inherent structures in water.[18] Previous quantum chemical studies of isotope fractionation in solution have been based on a limited number of solute−solvent conformations without any methodical way of searching for conformers. This approach might not recover the potential diversity of conformations present in the system, potentially biasing the results of the calculations to the particular conformations chosen to represent the system. An important aspect of our study is the extraction of *multiple* solvent−solute conformations from DFT-MD simulations, giving a better understanding of the error inherent in the supermolecule approach to estimating isotopic fractionation factors. Second, we introduce a new method of representing crystalline systems with molecular clusters based on conservation of Pauling bond strength. Our method increases the flexibility of using molecular codes for calculations of models of solid-state systems and allows relatively seamless integration of calculations on gas, aqueous, and solid-state systems.

II. Methods

II.A. Isotope Fractionation Calculations. To calculate the vibrational frequencies needed for determination of isotopic fractionation factors, one can use empirical force field approaches or electronic structure methods to calculate the necessary second and possibly higher derivatives. For this study, we use DFT[19] and molecular orbital theory with correlation treated at the second-order Møller−Plesset (MP2) level[20,21] to predict the vibrational frequencies. The accuracy of the results will depend on the approach used to calculate the electronic structure, the basis set, and the choice of the model system, in this case: (i) a single molecule with continuum solvent, (ii) the solute with an explicit first solvation shell embedded in continuum solvent, and (iii) the solute with explicit first and a (partial) second solvation shell.

Given the harmonic frequencies of the minimum-energy structure one can calculate the partition functions needed to predict carbon-isotope fraction. The reduced partition function ratio (RPFR) (or β) in the harmonic approximation is given by

$$\beta = \left(\frac{Q_h}{Q_l}\right) = \prod_i \frac{u_{hi}}{u_{li}} \frac{e^{-u_{hi}/2}}{1 - e^{-u_{hi}}} \frac{1 - e^{-u_{li}}}{e^{-u_{li}/2}} \qquad (1)$$

where $u_{(h,l)i} = \hbar c 2\pi\omega_{(h,l)i}/k\mathrm{T}$. The $\omega_{(h,l)i}$ are the frequencies (usually in cm^{-1}) for the heavy (h, ^{13}C) and light (l, ^{12}C) isotopes and the product extends over all characteristic frequencies of the molecule or supermolecule.[22,23] The equilibrium isotope fractionation factor (IFF) between species i and j is then given by $\alpha_{ij} = \beta_i/\beta_j$. $\alpha_{ij} > 1$ means that the heavy isotope is concentrated in species i. In referring to fractionation factors it is convenient to use the standard "ϵ_{ij}" notation where $\epsilon_{ij} = (\alpha_{ij} - 1) \times 1000$. The calculated results for comparison to experiment depend on the quality of the harmonic frequencies, which depend on the computational method, and the approximation that the isotope fractionation factor depends only on the harmonic frequencies. There is an extensive literature on the calculation of vibrational frequencies that we do not review here.

The Redlich−Teller product rule[24] for isotope effects in harmonic vibrational frequencies must be obeyed by any set of harmonic vibrational frequencies:

$$\frac{3}{2}\ln\left(\frac{M'}{M}\right) + \frac{3}{2}\ln\left(\frac{m}{m'}\right) = \sum_i \ln\frac{\omega_i'}{\omega_i} \qquad (2)$$

where M' (M) refers to the mass of the molecule containing the isotopically light (heavy) atom, m' (m) refers to the atomic mass of the isotopically light (heavy) atom, and the ω'_i (ω_i) are the light (heavy) harmonic frequencies which we predict from our electronic structure calculations. For CO_2, for example, taking the ^{12}C mass of 12.00000, the ^{13}C mass of 13.00335, and the ^{16}O oxygen mass of 15.99491, the left-hand side is equal to 0.08662. The sum of the logarithms of the ratios of the light isotope frequencies to the heavy isotope frequencies, over all the harmonic normal modes, must be equal to 0.08662 for any harmonic potential for CO_2. For quantum mechanical calculations of harmonic frequencies for small molecules, adherence to the Redlich−Teller rule is not a major issue. However, for calculations on larger molecular systems, and with continuum solvent models with numerical Hessians, the Redlich−Teller product provides insight into the quality of the calculations and is a test of the quality of the reduced partition function ratio.

II.B. Aqueous Species. The simplest approach to the prediction of IFFs is to calculate the frequencies of the individual molecules or ions either as isolated species or with a self-consistent reaction field (SCRF) approach[25] to model the solvent. The geometry is optimized and the second derivatives of the energy with respect to the nuclear coordinates are evaluated in the continuum solvent to obtain the vibrational frequencies in the harmonic approximation as well as the normal modes.

For the small-molecule/SCRF calculations, we used the Gaussian03 software[26] at the DFT and molecular orbital theory MP2 levels. For the DFT calculations, we chose the pure DFT exchange−correlation functionals PBE,[27] PW91,[28,29] and BP86,[30,31] as well as the B3LYP[32,33] hybrid functional as implemented in Gaussian03. The augmented, correlation-consistent aug-cc-pVDZ basis set,[34] which contains diffuse functions for the accurate treatment of anions, was used for these calculations. For the SCRF, calculations were done with the polarizable continuum models PCM, CPCM, and IEFPCM[35] as implemented in Gaussian03, and with the COSMO model[36] as implemented in the PQS software.[37]

An improved structural model is to embed the solute (CO_2, HCO_3^-, CO_3^{2-}) in a number of water molecules to form a so-called "supermolecule", find a stationary structure with zero forces, and calculate the second derivatives (see refs 12 and 38 for application of this method to isotope fractionation in the aqueous boron system). The main computational bottleneck in this approach is the generation of independent representative solvent−solute configurations and subsequent optimization of the large supermolecular clusters at a reasonable level of theory. We use DFT-MD simulations as an efficient way to generate representative configurations sampling important areas of the potential energy surface for subsequent study. After extraction of these configurations from the DFT-MD trajectories, they are optimized to a local minimum-energy configuration. Recent advances in optimization techniques for molecular clusters[39] can substantially reduce the time needed for energy minimization which can be difficult due to the significant number of floppy modes. The use of DFT-MD to generate appropriate starting configurations allows the calculation of isotopic fractionation for not just a single cluster, but for many minimum-energy

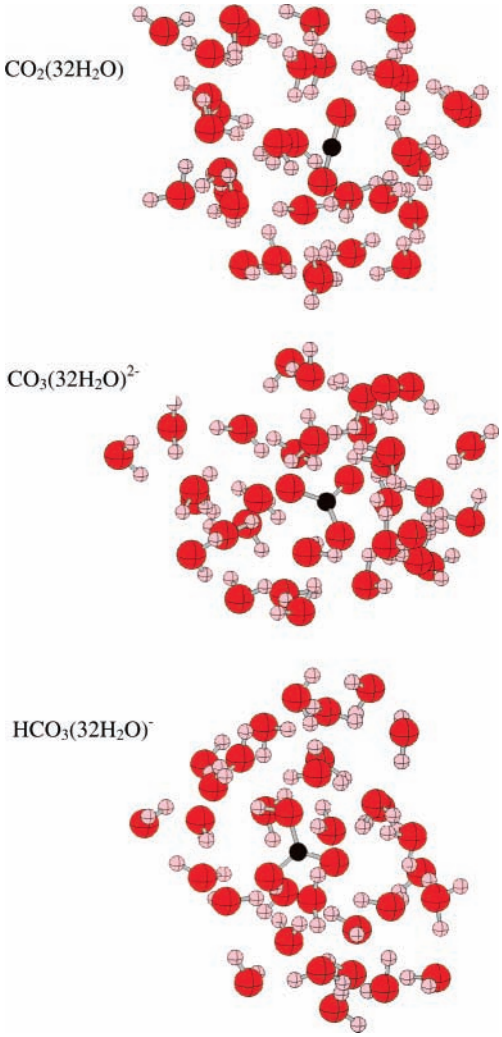

Figure 1. Representative 32-water clusters for CO_2(aq), CO_3^{2-}(aq), and HCO_3^-(aq). Oxygen atoms are red, protons are pink, and carbon is black.

conformations of the distribution of water molecules around the solutes. The presence of multiple conformations provides a means of assessing the errors introduced due to accessible stationary solvent configurations that are close to (but not exactly at) the global minimum energy.

DFT-MD simulations were carried out using the method of Car and Parrinello[40] as implemented in NWChem release 4.7.[41,42] Pseudopotentials were taken from Troullier and Martins.[43] We used the PBE exchange−correlation functional[27] with an energy cutoff of 90 au (atomic units = 1 hartree ≈ 627.5 kcal/mol) for the plane-wave basis. The fictitious mass μ was set at 400 au, and the time step set at 3 au (7.26×10^{-17} s). Electronic and nuclear degrees of freedom were attached to separate Nose−Hoover thermostats at 150 and 300 K, respectively. The mass parameter for both thermostats was set to 250 au.[44] To check the potential size dependence of the DFT-MD results for the ionic systems, we carried out calculations on systems with both 32 and 64 water molecules. For The CO_2-(aq) system we used only 32 water molecules.

In obtaining the IFFs, we limit our calculations to the 32-water systems. Fifteen configurations for each species, consisting of 32 water molecules and one solute molecule, were extracted from the DFT-MD trajectories at 1 ps intervals near the end of production runs (see representative structures in Figure 1). Atom coordinates were shifted to place the carbon atom of the solute molecule at the center of the repeating cell. The periodic boundary conditions were then removed, and the configurations were optimized in the gas phase using the PQS quantum chemistry package version 3.3.[37] We used the 6-31G* Gaussian basis set with the same PBE and B3LYP exchange−correlation functionals described above. For the ionic species, we also investigated smaller supermolecular clusters $HCO_3 \cdot 7H_2O^-$ and $CO_3 \cdot 9H_2O^{2-}$, taking just the first solvation shell obtained from the DFT-MD trajectories. For some of these calculations, we estimated the effects of the second- and larger-shells using SCRF methods. We used both COSMO as implemented in PQS and PCM as implemented in Gaussian03. For selected systems, we also present results using the aug-cc-pVDZ basis set.

Geometry optimization of the large 32-water clusters was carried out in delocalized cluster coordinates[39] using the eigenvector-following algorithm[45] and the default settings in the PQS code. To accelerate the initial optimization from the configurations generated by DFT-MD at 300 K, we used the Fourier-transform Coulomb (FTC) method[46] with the PBE functional and the 6-31G* basis set. After the PBE-FTC optimizations were complete, the configurations were re-optimized with the B3LYP functional (without the FTC method). In one or two configurations for each species, the solute molecule migrated to the outside of the cluster during optimization. These conformations were not considered in the subsequent analysis.

At least 13 usable configurations were produced for each species. Our final results are not weighted according to the energy of the associated conformer because artificial surface effects could influence energetic differences. If the RPFR values were Boltzmann-weighted, there would be even less variation in the fractionation factors. Therefore, the statistical uncertainties in the RPFR values for the aqueous species are probably overestimated in our approach.

II.C. Carbonate Minerals. We introduce here a general method that enhances the flexibility of molecular clusters to represent molecular environments in extended crystalline systems. The method, which we will refer to as the Pauling bond strength (PBS)-conserving termination method, is guaranteed to generate a neutral, autocompensated cluster. Clusters were extracted from known $CaCO_3$ (aragonite),[47] $CaCO_3$ (calcite),[48] $CaMg(CO_3)_2$ (dolomite),[49] and magnesite $MgCO_3$ (magnesite)[48] crystal structures, with the origin set at a central carbonate unit (see Figure 2). The clusters were constructed by incorporating all Ca, Mg centered polyhedra sharing oxide ions with the central carbonate. In turn, all carbonate groups attached to the calcium/magnesium polyhedral units were extracted and kept whole. Broken bonds between the oxide ions of the second carbonate shell and external calcium/magnesium ions were saturated with "link" atoms placed 1 Å from the oxide ion along the broken Ca, Mg−O bond. The charges of the link atoms are set equal to the Pauling bond strength (charge/coordination number) of the "removed" metal ion. For the rhombohedral carbonates calcite, dolomite, and magnesite where the divalent cations are in octahedral coordination, the charge is 2/6; for aragonite, where calcium is 9-fold coordinated, it is 2/9.

Our algorithmic approach removes much of the arbitrariness involved in terminating such a cluster with hydrogen atoms with a full nuclear charge because it is not necessary to decide which terminating groups get hydrogen atoms and at the same time satisfying charge neutrality constraints. Simply terminating the cluster with hydrogens of full charge can give clusters with large positive charges that are unphysical and can even lead to SCF convergence problems as well as issues with geometry optimizations.

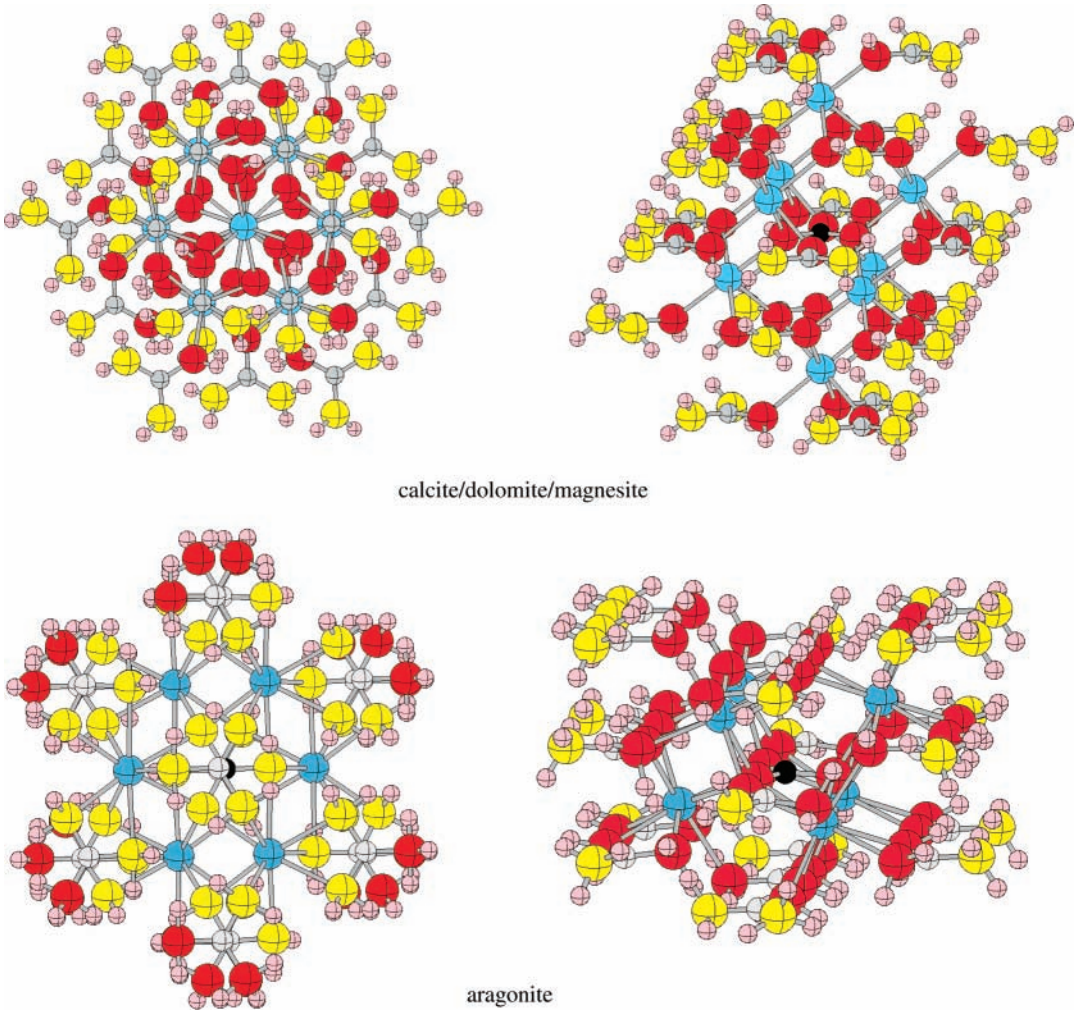

Figure 2. Clusters for rhombohedral and orthorhombic carbonate phases. The position of the black carbon atom and positions of the red oxide ions and divalent metal ions (Ca,Mg; blue) are fully optimized and included in the harmonic frequency calculations. Gray carbon atoms and yellow oxygen atoms are fixed in their experimental lattice positions and excluded from the frequency calculations. Link atoms are pink and have a +2/6 charge for the rhombohedral carbonates (calcite, dolomite, magnesite), and a +2/9 charge for the aragonite.

The 3-21G basis set for hydrogen was assigned to the link atoms. The 3-21G basis set was used for all C nuclear centers (except at the central carbonate) and for all oxide ions not attached to calcium/magnesium metal centers. The 6-31G* basis set was assigned to all calcium/magnesium metal centers, all oxide ions attached to the divalent metal centers, and to the central carbonate group. All atoms and link atoms with 3-21G basis functions were held fixed while the positions of the rest of the atoms were optimized according to the criteria above.

Vibrational frequencies for ^{12}C and ^{13}C centered clusters were calculated from an analytical Hessian restricted to the optimized atoms. The partial block Hessian matrix was diagonalized using the Jacobi method to find the frequencies and normal modes. One must take care to avoid projecting out the translational and rotational degrees of freedom, as this is not appropriate for an embedded cluster and is often done automatically in quantum chemistry codes. Similar partial Hessian techniques have been described previously.[50] RPFR values were then calculated by applying a modified version of eq 1 without the leading u_{hi}/u_{li} ratio as in a crystal there are no rotational/translational terms. The RPFRs for the mineral species were numerically extrapolated to infinite temperature, and the limiting value of β as $T \rightarrow \infty$ value was divided into $\beta(T)$ to recover the proper high-temperature limit.[51]

III. Results

III.A. Aqueous Species with Continuum Solvent. The first set of calculations was done on gas-phase CO_2, H_2CO_3, HCO_3^-, and CO_3^{2-} as well as these molecules/ions embedded in solvent modeled by a SCRF. The calculated bond distances for the neutral species are shown in Table 1 (bond distances for the ionic species are given in the Supporting Information). For CO_2, the C═O bond distance ranges from 1.167 to 1.180 Å in the gas phase. The shortest value is at the B3LYP level and the longest is at the MP2 level. The PBE functional predicts bond distances slightly shorter than the MP2 value. The calculated bond distances are all longer than the experimental value of 1.1621 Å. The inclusion of a solvation model does little to affect the calculated bond distances.

The H_2CO_3 molecule has C_{2v} symmetry with a short C═O bond and two long C−O bonds. The C═O bond distances vary from 1.210 (B3LYP) to 1.222 (BP86) Å and the C−O bond distances vary from 1.343 (B3LYP) to 1.357 (BP86) Å. The SCRF lengthens the C═O bond distance by about 0.01 Å and shortens the C−O bond distance by a comparable amount. The C_s structure, generated by rotation about one C−O(H) bond, is of higher energy.

HCO_3^- is predicted to have one long C−O bond involving the O bonded to the H atom and two shorter C−O bonds which differ by about 0.02 Å in the gas phase. The long C−O bond

TABLE 1: Bond Lengths *R* (Å) for Neutral Species CO_2 and H_2CO_3 at Various Levels of Theory Using the aug-cc-pVDZ Basis Set

bond distance	method	gas (*R*)	SCRF(R)
	CO_2		
C═O	B3LYP	1.1673	1.1670
C═O	MP2	1.1802	1.1791
C═O	PBE	1.1787	1.1781
C═O	PW91	1.1776	1.1797
C═O	BP86	1.1796	1.1790
	H_2CO_3		
C═O	B3LYP	1.2104	1.2200
C═O	B3LYP	1.3437	1.3354
O−H	B3LYP	0.9690	0.9929
C═O	MP2	1.2180	1.2256
C−O	MP2	1.3507	1.3426
O−H	MP2	0.9712	0.9968
C═O	PBE	1.2212	1.2300
C−O	PBE	1.3549	1.3466
O−H	PBE	0.9782	1.0043
C═O	PW91	1.2201	1.2287
C−O	PW91	1.3535	1.3456
O−H	PW91	0.9773	1.0033
C═O	BP86	1.2223	1.2308
C−O	BP86	1.3567	1.3489
O−H	BP86	0.9792	1.0054

distance is 0.10−0.12 Å longer than in H_2CO_3. The short CO_2 bond distances within the delocalized CO_2^- moiety in the anion are 0.03−0.05 Å longer than in H_2CO_3. Again, the B3LYP functional predicts the shortest bond lengths and BP86 predicts the longest bond lengths. The inclusion of solvation effects at the SCRF level dramatically shortens the long C−O bond distance by almost 0.05 Å and makes the CO_2^- moiety have approximately equal bond lengths by lengthening the short C═O bond distance more than the longer C═O bond distance in the CO_2^- fragment.

The bond distance in CO_3^{2-} lengthens from that in the CO_2^- fragment in HCO_3^- by about 0.06 Å. Again, the B3LYP functional predicts the shortest bond distance and the BP86, the longest bond distances. Inclusion of the SCRF shortens the C−O bond distance in CO_3^{2-} by 0.01 Å.

The calculated frequencies for CO_2 and H_2CO_3 are given in Table 2; those for HCO_3^- and CO_3^{2-} are given in the Supporting Information. For CO_2(g), the experimental frequencies including anharmonicity[52] are 2349.16, 1288.17, and 667.40 cm^{-1}. The experimental harmonic frequencies[53,54] are $^{12}C^{16}O_2$ ($^{13}C^{16}O_2$), 2396.30 (2328.03), 1353.62 (1353.62), and 672.83 (653.72) cm^{-1}. The experimental values for ω are matched by the calculated values at the B3LYP level to within ten cm^{-1}. The calculated values all lie below the measured values. The MP2 values are quite close to experiment for the asymmetric stretch and the bend but are too low by almost 50 cm^{-1} for the symmetric stretch at the aug-cc-pVDZ level. The other functionals all predict frequencies that are too low and show errors of up to 60 cm^{-1} for the asymmetric stretch. The effect of the solvent at the SCRF level is to substantially decrease the asymmetric stretch. The symmetric stretch increases by different amounts dependent on the SCRF approach. The bend is predicted to decrease on solvation. The largest isotopic shift is found for the asymmetric stretch.

Table 3 gives the reduced partition function ratios (RPFRs, β in eq 1) for the unsolvated and SCRF-solvated species. It should be emphasized that we do not apply scaling factors to the calculated frequencies because the scaling factors, in part, correct for vibrational anharmonicity. Because we are using a harmonic partition function to predict the isotope fractionation, it is appropriate to use harmonic frequencies as input (see discussion in ref 14). For both the DFT and MP2 Hamiltonians and all continuum solvation models (PCM, CPCM, IEFPCM), the RPFR values of the ionic species are much smaller than the CO_2(g), making the solvated ions isotopically light relative to CO_2(g), in contradiction to experiment. Hence, IFFs cannot be predicted on the basis of a single ionic species with the SCRF solvation model; at least some explicit waters of solvation are needed to correctly predict even the sign of the carbon-isotope fractionation factors in aqueous systems. Although the SCRF approach performed poorly when diffuse basis functions are used, we carried out some (unreported) calculations, indicating that better results are obtained with the 6-31G* basis. Because we are interested in anions, which are known to be better treated with diffuse functions in the basis set, we did not pursue this issue further, as the improvement with the less robust basis set is probably accidental. All of the pure DFT functionals (PBE, PW91, BP86) give very similar results with smaller RPFRs than obtained with the B3LYP and MP2 Hamiltonians. As shown in Table 3, the MP2-PCM combination yielded harmonic frequencies deviating significantly from the Redlich-Teller product.

III.B. Aqueous Species with Explicit Waters of Solvation. To include specific waters of solvation, we took configurations generated from the DFT-MD simulations. The C−O and C−H radial distribution functions from the periodic Car−Parrinello DFT-MD calculations for the species CO_2(aq), HCO_3^-(aq), and CO_3^{2-}(aq) are shown in Figure 3. Nonpolar CO_2(aq) is poorly hydrated with a small preference for the hydrogen end of the water molecules to be oriented toward the oxygen. The charged species, bicarbonate and carbonate, as expected, are more strongly hydrated. HCO_3^-(aq) has a hydration shell of 7−8 water molecules with 3−4 hydrogen bonds formed between the oxygen atoms of the bicarbonate ion and the hydrogen atoms from the solvating water molecules. The carbonate ion has a hydration shell of ∼9−10 water molecules and accepts, on average, ∼8 hydrogen bonds from the surrounding solvent. The overall system-size dependence of the structure of the first shell is small, but particularly for bicarbonate, the variability of the first shell appears larger in the 32-water system than in the 64-water system. The 64-water systems display a small but reproducible second-shell peak near 5.5 Å. This feature is better developed in the bicarbonate system than in the carbonate system. Each trace of the radial distribution function in Figure 3 represents a separate simulation of 6 ps.

The RPFRs predicted from the supermolecule vibrational frequencies with the PBE and B3LYP functionals at 25 °C are given in Table 4. For the $HCO_3{\cdot}7H_2O^-$ and $CO_3{\cdot}9H_2O^{2-}$ (used to model a single solvation shell) we report results for both the 6-31G* and aug-cc-pVDZ basis sets. For the larger $CO_2{\cdot}32H_2O$, $HCO_3{\cdot}32H_2O^-$, and $CO_3{\cdot}32H_2O^{2-}$ clusters, we only include results for multiple conformers with the 6-31G* basis set. We also provide calculations for single conformers of $HCO_3{\cdot}32H_2O^-$ and $CO_3{\cdot}32H_2O^{2-}$ at the B3LY/aug-cc-pVDZ level. The carbon-isotope fractionation factors in $\epsilon_{bicarbonate-CO_2(g)}$, $\epsilon_{carbonate-CO_2(g)}$, and $\epsilon_{CO_2(aq)-CO_2(g)}$ notation, are given in Table 5 at 25 °C and are shown as a function of temperature in Figure 4, where they are compared to the expressions derived from isotopic fractionation measurements given in ref 4. The temperature dependences of $\epsilon_{bicarbonate-CO_2(g)}$ and $\epsilon_{carbonate-CO_2(g)}$ are very similar and consistent with experimental measurements.

The results in Tables 4 and 5 reveal a complicated dependence of the calculated RPFRs and IFFs on the size of the cluster, the functional, and the basis set. For the solvated species, the RPFRs

TABLE 2: Vibrational Frequencies (cm^{-1}) for Neutral Species CO_2 and H_2CO_3 at Various Levels of Theory Using the aug-cc-pVDZ Basis Set (aug-cc-pVTZ Results Also Included for CO_2(g) for B3LYP and MP2 Hamiltonians)

	gas		PCM	
CO_2	^{12}C	^{13}C	^{12}C	^{13}C
experiment[53,54]				
C═O asymm stretch	2396.30	2328.03		
C═O symm stretch	1353.65	1353.62		
O═C═O bend	672.83	653.72		
B3LYP				
C═O asymm stretch	2388.8	2320.9	2338.9	2272.3
C═O symm stretch	1354.5	1354.5	1356.1	1356.1
O═C═O bend	666.6	647.6	659.1	640.4
B3LYP (aug-cc-pVTZ)				
C═O asymm stretch	2399.6	2331.5		
C═O symm stretch	1368.5	1368.5		
O═C═O bend	673.7	654.6		
MP2				
C═O asymm stretch	2379.5	2311.8		
C═O symm stretch	1305.5	1305.5		
C═O═O bend	655.4	636.8		
MP2 (aug-cc-pVTZ)				
C═O asymm stretch	2401.6	2333.5		
C═O symm stretch	1325.8	1325.8		
O═C═O bend	658.6	639.9		
PBE				
C═O asymm stretch	2343.9	2277.2	2303.0	2237.5
C═O symm stretch	1307.5	1307.5	1309.8	1309.8
O═C═O bend	639.6	621.4	633.4	615.4
PW91				
C═O asymm stretch	2343.6	2276.9	2302.4	2236.8
C═O symm stretch	1308.7	1308.7	1311.0	1311.0
O═C═O bend	639.9	621.7	633.7	615.7
BP86				
C═O asymm stretch	2331.2	2264.9	2290.2	2225.0
C═O symm stretch	1301.5	1301.5	1303.8	1303.8
O═C═O bend	638.2	620.0	632.0	614.1

	gas		PCM	
H_2CO_3	^{12}C	^{13}C	^{12}C	^{13}C
B3LYP				
O−H symm stretch	3788.6	3788.6	3265.0	3265.0
O−H asymm stretch	3786.0	3786.0	3248.9	3248.8
C═O stretch/O−H symm bend	1816.0	1770.4	1724.6	1680.5
C−O asymm stretch/O−H asymm bend	1453.8	1421.7	1419.2	1387.8
O−H symm bend	1294.9	1294.7	1255.8	1255.8
C−O asymm stretch/O−H asymm bend	1163.7	1155.6	1135.2	1127.9
C−O symm stretch	971.9	969.7	987.9	985.8
CO_3 inv	791.6	767.8	790.6	765.9
C═O−O bend	602.7	601.7	593.9	592.0
O−C−O bend	594.7	593.1	565.4	563.1
O−H asymm bend	541.7	539.4	541.8	541.7
O−H asymm bend	534.3	534.3	468.2	468.2
MP2				
O−H symm stretch	3788.7	3788.7	3216.6	3216.6
O−H asymm stretch	3786.9	3786.8	3200.6	3200.5
C═O stretch/O−H symm bend	1815.5	1769.7	1733.1	1689.4
C−O asymm stretch/O−H asymm bend	1452.6	1420.7	1409.9	1379.2
O−H symm bend	1295.5	1295.3	1258.4	1258.4
C−O asymm stretch/O−H asymm bend	1166.5	1158.3	1139.0	1131.9
C−O symm stretch	965.3	963.3	989.5	987.6
CO_3 inv	788.8	764.9	783.4	761.2
C═O−O bend	606.1	605.4	610.4	608.8
C−O−O bend	593.8	592.1	579.6	577.4
O−H symm bend	542.6	540.3	518.9	518.8
O−H asymm bend	536.8	536.8	445.3	445.3
PBE				
O−H symm stretch	3672.5	3672.5	3117.3	3117.3
O−H asymm stretch	3669.4	3669.4	3101.7	3101.5
C═O stretch/O−H symm bend	1766.1	1721.8	1683.4	1640.3
C−O asymm stretch/O−H asymm bend	1406.8	1375.9	1373.3	1343.3
O−H symm bend	1253.2	1253.0	1216.7	1216.7
C−O asymm stretch/O−H asymm bend	1117.9	1110.1	1093.2	1085.9
PBE (cont'd)				
C−O symm stretch	938.9	936.8	954.8	952.9
CO_3 inv	757.0	734.3	757.6	733.9
C═O−O bend	594.0	593.1	570.2	568.4
C−O−O bend	570.4	568.8	544.6	542.3
O−H symm bend	520.9	520.9	535.6	535.5
O−H asymm bend	520.0	517.7	458.4	458.4
PW91				
O−H symm stretch	3676.2	3676.1	3123.7	3123.7
O−H asymm stretch	3673.0	3673.0	3108.1	3107.9
C═O stretch/O−H symm bend	1765.1	1720.8	1682.9	1639.8
C−O asymm stretch/O−H asymm bend	1408.4	1377.5	1373.1	1343.1
O−H symm bend	1253.7	1253.5	1215.7	1215.6
C−O asymm stretch/O−H asymm bend	1118.2	1110.3	1091.5	1084.2
C−O symm stretch	940.4	938.3	955.2	953.3
CO_3 inv	757.6	734.9	758.1	734.4
C═O−O bend	593.3	592.4	570.5	568.7
C−O−O bend	570.6	569.0	544.8	542.5
O−H symm bend	520.9	520.9	533.3	533.2
O−H asymm bend	520.8	518.5	456.2	456.2
BP86				
O−H symm stretch	3659.9	3659.9	3103.4	3103.4
O−H asymm stretch	3657.0	3657.0	3088.0	3087.9
C═O stretch/O−H symm bend	1756.3	1712.3	1674.3	1631.5
C−O asymm stretch/O−H asymm bend	1402.4	1372.0	1366.2	1336.9
O−H symm bend	1251.4	1251.2	1213.6	1213.6
C−O asymm stretch/O−H asymm bend	1113.4	1105.2	1086.4	1078.7
C−O symm stretch	933.2	931.1	947.5	945.6
CO_3 inv	754.1	731.5	754.8	731.2
C═O−O bend	590.5	589.6	568.0	566.2
C−O−O bend	568.1	566.5	542.1	539.9
O−H symm bend	518.0	516.4	529.6	529.5
O−H asymm bend	516.4	515.8	451.4	451.4

calculated with B3LYP are consistently 10 per mil more positive than those calculated with PBE, regardless of the size of the solvation shell (this is also true of the calculations with no explicit waters of solvation described above and shown in Table 3). For CO_2(g), the RPFR predicted by the B3LYP functional is also larger than that predicted by the PBE functional, but the difference is smaller than that of the solvated species. Second, for both functionals, increasing the size of the solvent shell from 7 or 9 waters to 32 water molecules increases the RPFRs by 4−5 per mil for the carbonate ion and 2−3 per mil for the bicarbonate ion. Third, for the two ions, when the basis set is improved from 6-31G* to aug-cc-pVDZ, there is a 4−6 per mil decrease in the RFPRs for both functionals using the single solvent shell model. In contrast, for CO_2(g), the RPFR predicted with the improved basis set is somewhat *larger* than with the 6-31G* basis set. This difference is due to the different types of interactions that dominate the intermolecular energetics. For the solvated ions, the intermolecular interactions are dominated by strong hydrogen bonds which, of course, are not relevant for CO_2(g). On the other hand, the increase in the RPFR for CO_2(g) with the larger basis set is still significant. The larger basis set improves the description of the C═O bond as well as providing a better description of hydrogen bonding in the solvent. As shown in Tables 4 and 5, that MP2/aug-cc-pVDZ calculations of the IFFs are very close to the B3LYP/aug-cc-pVDZ calculations.

The dependence of the RPFR on conformation for the PBE/6-31G* 32-water clusters is given in Table 6. The calculations show that errors could be introduced by ignoring the conformational dependence of the RPFRs. Considering the standard error on ∼10 conformers, the conformation problem is manageable and is smaller than the systematic errors associated with

TABLE 3: Reduced Partition Function Ratios at 25 °C Calculated Using the aug-cc-pVDZ Basis Set at DFT (Using B3LYP, PBE, PW91, BP86 Exchange−Correlation Functionals) and the MP2 Levels

	gas	PCM	CPCM	IEFPCM	COSMO[a]
			CO_2		
B3LYP	1.1935	1.1885	1.1885	1.1885	1.1887
B3LYP[b]	1.1948				
MP2	1.1914	1.1806 (0.0800)[c]	1.1808	1.1806	1.1839
MP2[b]	1.1930				
PBE	1.1864	1.1824	1.1822	1.1822	
PW91	1.1864	1.1824	1.1822	1.1824	
BP86	1.1852	1.1810	1.1810	1.1810	
expt[7]	1.1943 (1.1910)[d]				
			H_2CO_3		
B3LYP	1.2099	1.2016	1.2019	1.2016	
MP2	1.2098	1.1943 (0.0911)	1.1943	1.1943	
PBE	1.1988	1.1918	1.1919	1.1921	
PW91	1.1993	1.1920	1.1918	1.1920	
BP86	1.1972	1.1896	1.1901	1.1896	
			HCO_3^-		
B3LYP	1.1874	1.1860	1.1861	1.1860	1.1846
MP2	1.1855	1.1761 (0.0900)[c]	1.1762	1.1761	1.1806
PBE	1.1763	1.1756	1.1749	1.1756	
PW91	1.1764	1.1758	1.1755	1.1758	
BP86	1.1746	1.1738	1.1740	1.1737	
			CO_3^{2-}		
B3LYP	1.1756	1.1809	1.1809	1.1809	1.1830
MP2	1.1721	1.1679 (0.0905)[c]	1.1680	1.1679	1.1760
PBE	1.1613	1.1700	1.1697	1.1700	
PW91	1.1616	1.1701	1.1702	1.1701	
BP86	1.1593	1.1682	1.1680	1.1679	

[a] COSMO model as implemented in PQS. [b] Calculation done with the aug-cc-pVTZ basis set. [c] MP2 continuum solvation model does not obey the Redlich−Teller product rule, value given in parentheses is $\Sigma\ln(\omega_i/\omega_i')$. [d] Experimental harmonic(anharmonic) from ref 7.

the basis set and Hamiltonian. However, if only a single configuration had been chosen to represent the system, there would have been a reasonable chance of obtaining a value differing 2−3 per mil from the average value. With 13 configurations, the standard error in the mean is approximately 0.3−0.4 per mil.

We also report the Redlich-Teller products for the large 32-water clusters. For the smaller systems, the Redlich−Teller products were all within 0.00001 of their target value (except for the MP2-PCM combination mentioned above). For the larger systems, the standard error is close to 0.0001. It is possible that this error could be improved by tightening convergence tolerance on the geometry optimization and, for the DFT calculations, improving the size of the grid. This was not explored here; the average Redlich−Teller products are very close to their required values, and there is no correlation between the RPFR and the Redlich−Teller product. However, the deviation could become more important as higher accuracies are desired. For the CO_2-(aq) configurations, three of the Redlich−Teller products are in the 0.112 range. These configurations are not included in the average RPFR. The anomalous results for those three conformers, obtained using the same procedures as all the other conformers, underscore the importance of checking the Redlich−Teller product for each calculated RFPR.

The combination of the shifts in RPFRs just described leads to systematic variations in the calculated IFFs. For the 6-31G* basis set, the values of $\epsilon_{HCO_3^-/CO_2(g)}$ and $\epsilon_{CO_3^{2-}/CO_2(g)}$ calculated

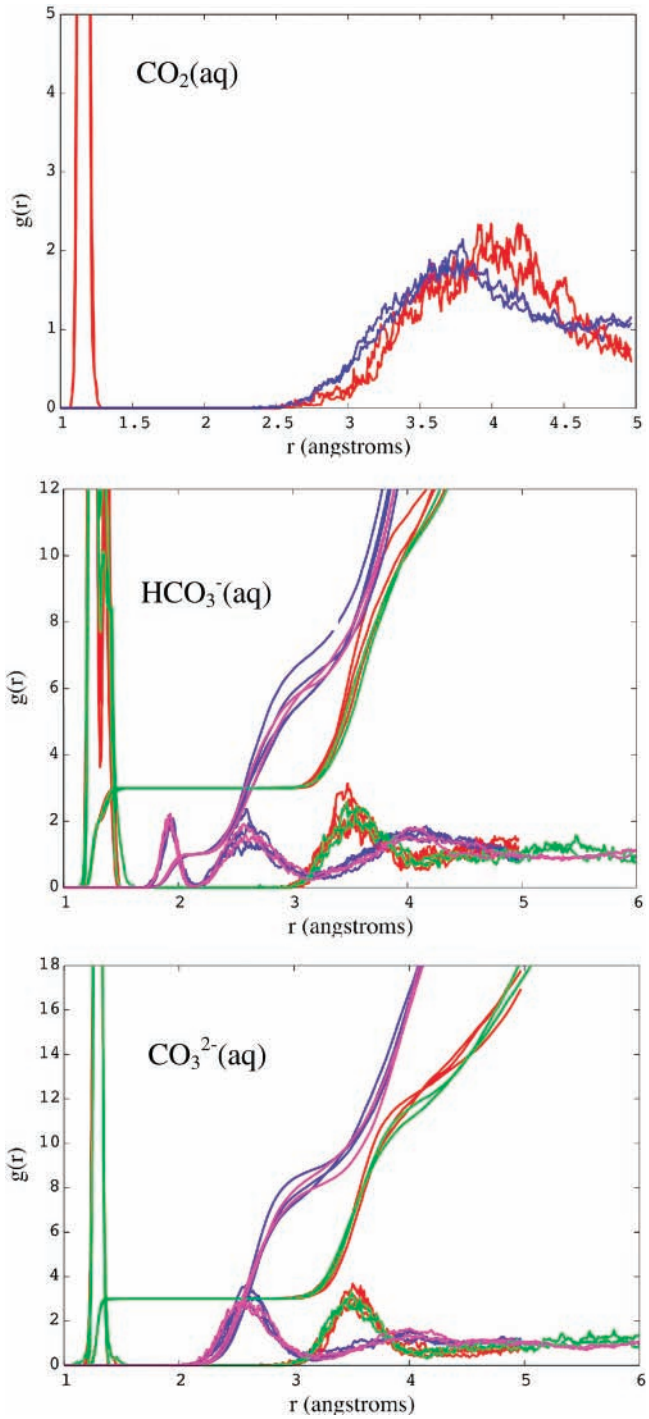

Figure 3. Radial distribution function and running coordination numbers of hydrogen (blue, 32 H_2O system; purple, 64 H_2O system) and oxygen (red, 32 H_2O; green, 64 H_2O) about the central carbon atom in (top) bicarbonate, (middle) carbonate, and (bottom) carbon dioxide in the periodic Car−Parrinello calculations using the PBE exchange−correlation functional. Each line represents a trial 6 ps calculation.

with PBE are 4−5 per mil lower than those calculated with B3LYP. There is some evidence that this difference may be smaller when the aug-cc-pVDZ basis is used, but because we did not perform PBE/aug-cc-pVDZ calculations for any of the 32-water clusters, the suggestion is somewhat speculative. The basis set has a large effect on the predicted IFFs for the ionic species, with the aug-cc-pVDZ calculations being about 5−8 per mil lower than the 6-31G* calculations. For the ions,

TABLE 4: Reduced Partition Function Ratios (β's) for Aquo Ions (25 °C)

method	$CO_2 \cdot 32H_2O$	CO_2(g)	$CO_3 \cdot 32H_2O^{2-}$	$HCO_3 \cdot 32H_2O^-$
B3LYP/6-31G*	1.1917(2) [0.1169(3)][a]	1.1909	1.2064(3) [0.1178(1)]	1.2103(4) [0.1177(1)]
B3LYP/aug-cc-pVDZ[b]		1.1935	1.2015[c]	1.2036[c]
B3LYP/aug-cc-pVDZ[d]		1.1935	1.1991 [0.11767]	1.2036 [0.11853]
PBE/6-31G*	1.1823(5) [0.1173(2)]	1.1858	1.1957(3) [0.1174(1)]	1.1989(4) [0.1176(2)]
Empirical estimate for CO_3^{2-}(aq)[7]			1.1967	
Left hand side of eq 1[e]	0.117648554		0.117709226	0.117712946

method	CO_2(g)	$CO_3.9H_2O^{2-}$	$HCO_3\langle 7H_2O^-$
B3LYP/6-31G*	1.1909	1.2021(3)	1.2080(4)
B3LYP/aug-cc-pVDZ	1.1935	1.1972(3)	1.2013(3)
B3LYP/6-31G*/COSMO		1.2029	1.2014
B3LYP/6-31G*/CPCM		1.2020	1.2030
B3LYP/aug-cc-pVDZ/PCM		1.1966	1.1958
MP2/aug-cc-pVDZ	1.1914	1.2016	1.1994
PBE/6-31G*	1.1858	1.1925(3)	1.1966(3)
PBE/aug-cc-pVDZ	1.1864	1.1866(3)	1.1907(3)
PBE/6-31G*/COSMO		1.1917	1.1916
PBE/6-31G*/CPCM		1.1910	1.1923
PBE/aug-cc-pVDZ/PCM		1.1864	1.1857

[a] For the large systems, Redlich−Teller products are given (left-hand side of eq 2) in square brackets (with standard errors in parentheses if more than one configuration is included). [b] Estimated value. [c] Estimated by scaling the B3LYP/6-31G*//32H2O β value by [β-B3LYP/aug-cc-pVDZ//(7,9H2O)]/(β-B3LYP/6-31G*//(7,9H2O)]. [d] Single configuration. [e] $^3/_2 \ln(M'/M) + {}^3/_2 \ln(m/m')$ where M' (M) is the mass of the isotopically light (heavy) cluster and m' (m) is the mass of the isotopically light (heavy) carbon atom. In the calculations, oxygen mass taken as 15.9994, hydrogen as 1.00794, $^{12}C = 12.0$, $^{13}C = 13.0$.

TABLE 5: Fractionation Factors (25 °C, per Mil)

method	$\epsilon_{CO_2(aq)-CO_2(g)}$	$\epsilon_{HCO_3-CO_2(g)}$	$\epsilon_{CO_3-CO_2(g)}$
expt (ref 4)	-1.2 ± 0.05	7.93 ± 0.05	5.9 ± 0.5
PBE/6-31G*//32H$_2$O	-3.0 ± 0.4	11.0 ± 0.4	8.4 ± 0.3
B3LYP/6-31G*//32H$_2$O	0.7 ± 0.2	16.3 ± 0.3	13.0 ± 0.3
B3LYP/aug-cc-pVDZ//32H$_2$O[a]		8.5 (estim)	7.1 (estim)
B3LYP/aug-cc-pVDZ//32H$_2$O		8.5 (1 conf)	4.8 (1 conf)
PBE/6-31G*/1st shell		9.1	4.0
PBE/aug-cc-pVDZ/1st shell		4.2	0.2
B3LYP/6-31G*/1st shell		13.7	9.4
B3LYP/aug-cc-pVDZ/1st shell		6.8	3.5
MP2/aug-cc-pVDZ/1st shell		6.7 (1 conf)	8.6 (1 conf)
B3LYP/aug-cc-pVDZ/PCM/1st shell		2.0	2.7
B3LYP/aug-cc-pVDZ/CPCM/1st shell		1.6	0.9
B3LYP/6-31G*/COSMO/1st shell		8.8	10.1
PBE/aug-cc-pVDZ/PCM/1st shell		0.1	−0.6
PBE/6-31G*/COSMO/1st shell		4.9	5.0

[a] Estimated by scaling the B3LYP/6-31G*//32H$_2$O β value by [β-B3LYP/aug-cc-pVDZ//(7,9H$_2$O)]/(β-B3LYP/6-31G*//(7,9H$_2$O)].

calculations on the 32-water system are 2−3 per mil higher than calculations including only the first solvation shell.

Rather than using a larger supermolecule to try to converge to the infinite-solvent limit, one can also use an SCRF approach to model the infinite solvent. Inclusion of an SCRF with the first solvent shell has the effect of reducing the RPFRs for HCO_3^-. For the dianion CO_3^{2-}, the results are less pronounced. With the B3LYP functional and the aug-cc-pVDZ basis set, the CO_3^{2-} RPFRs decrease. With the smaller 6-31G* basis set, the carbonate ion RPFRs slightly increases for both the B3LYP and PBE functionals. When the PBE functional is used with the aug-cc-pVDZ basis set, the RPFR for CO_3^{2-} decreases and now gives an incorrect sign for the IFF. The fact that the SCRF correction is much smaller than, or even opposite in sign to, the correction due to explicitly adding a second solvation shell suggests that one needs explicit waters beyond the first shell to get reliable results for the prediction of IFFs for these types of species.

The B3LYP/6-31G* calculation gives the wrong sense of fractionation between CO_2(aq) and CO_2(g), predicting that CO_2-(g) is isotopically lighter than CO_2(aq). The PBE/6-31G* calculations yield the correct sense of fractionation between CO_2-(g) and CO_2(aq) but with a larger fractionation than measured experimentally. We note that the interaction of CO_2 with H_2O will be dominated by van der Waals forces that are inherently not included in current DFT functionals. Furthermore, although absent from the plane-wave calculations of the hydration structure, basis set superposition error (BSSE) could play a role and we have not included this correction. The effect of BSSE is likely to be smaller on the frequencies than on the binding energies. We note that the experimental value for the IFF for CO_2 is near zero as predicted by both the B3LYP and PBE functionals within 3 per mil.

Figure 4 shows that the PBE exchange−correlation functional with the 6-31G* basis set predicts the qualitative sense of fractionation between CO_2(aq), CO_2(g), HCO_3^-(aq), and CO_3^{2-}(aq) as a function of temperature with a supermolecule model with 32 water molecules. The calculations with the PBE functional overestimate the fractionation between HCO_3^-(aq) and CO_2(g) by ~3 per mil. As shown in Table 5, the calculations

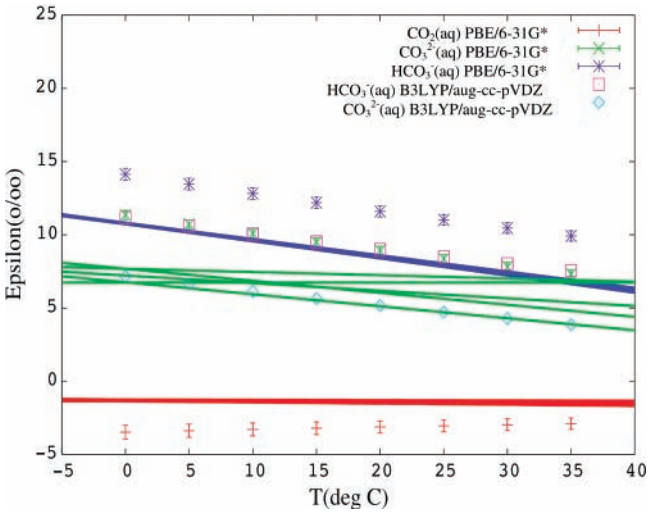

Figure 4. Temperature dependence of the predicted isotopic fractionation (per mil). Epsilon is defined as $(\alpha - 1) \times 1000$. All results are reported relative to CO_2(g) and are calculated from vibrational spectra on solute−solvent clusters with 32 water molecules at the PBE/6-31G* and B3LYP/aug-cc-pVDZ levels. There are no error bars on the B3LYP calculations because only a single conformer has been subject to calculations at that level. Solid lines are experimental measurements taken from ref 4 with uncertainties applied. Key: blue, HCO_3^-:CO_2(g); green, CO_3^{2-}:CO_2(g); red, CO_2(aq):CO_2(g). Note that the B3LYP/aug-cc-pVDZ results for HCO_3^- lie fortuitously almost exactly on top of the PBE/6-31G* results for CO_3^{2-}.

TABLE 6: Sorted RPFR Values (25 °C), and Associated Redlich−Teller Products (Left-Hand Side of Eq 2) in Parentheses, Calculated with PBE/6-31G* for Each of the Thirteen 32-Water Conformations

$CO_2 \cdot 32H_2O$	$CO_3 \cdot 32H_2O^{2-}$	$HCO_3 \cdot 32H_2O^-$
1.1790 (0.1166)	1.1936 (0.1182)	1.1959 (0.1180)
1.1799 (0.1182)	1.1939 (0.1165)	1.1970 (0.1169)
1.1803 (0.1172)	1.1943 (0.1183)	1.1973 (0.1173)
1.1808 (0.1127)[a]	1.1950 (0.1176)	1.1986 (0.1179)
1.1820 (0.1175)	1.1955 (0.1182)	1.1988 (0.1182)
1.1827 (0.1127)[a]	1.1958 (0.1180)	1.1989 (0.1181)
1.1830 (0.1179)	1.1958 (0.1183)	1.1989 (0.1167)
1.1832 (0.1177)	1.1959 (0.1171)	1.1991 (0.1178)
1.1833 (0.1162)	1.1964 (0.1171)	1.1992 (0.1173)
1.1835 (0.1172)	1.1965 (0.1175)	1.1995 (0.1171)
1.1838 (0.1172)	1.1966 (0.1169)	1.1999 (0.1176)
1.1839 (0.1123)[a]	1.1969 (0.1179)	1.2003 (0.1166)
1.1840 (0.1179)	1.1975 (0.1178)	1.2019 (0.1177)

[a] Conformer violates Redlich−Teller product rule. Fractionation factor not included in average in Table 4.

with the B3LYP functional and the 6-31G* basis on the supermolecule model with 32 water molecules perform significantly worse for the ionic species, overestimating the fractionation factors by ~7 per mil at 25 °C. Overall, the PBE/6-31G* calculations are superior to the B3LYP/6-31G* calculations for predicting isotope fractionation in these species in water.

On the basis of the B3LYP/6-31G* and B3LYP/aug-cc-pVDZ results for the $HCO_3 \cdot 7H_2O^-$ and $CO_3 \cdot 9H_2O^{2-}$ systems, we can estimate the reduction in the RFPR expected for the large system by taking β-B3LYP/6-31G*//($32H_2O$) × [β-B3LYP/aug-cc-pVDZ//($7,9H_2O$)]/(β-B3LYP/6-31G*//($7,9H_2O$)]. Estimates for the ionic species are given in Tables 4 and 5. The results differ by less than 1 per mil from the measured value for bicarbonate and differ by 1.2 per mil from the measured value for carbonate. Single conformers (with RPFRs near the average value) were chosen from the B3LYP/6-31G*//$32H_2O$ set for carbonate and bicarbonate. These were optimized at the B3LYP/aug-cc-pVDZ level and vibrational frequencies were calculated. For the single conformers, the actual RPFR for bicarbonate is very close to the estimated value. The actual RPFR for carbonate is more than 2 per mil below the estimated value.

TABLE 7: Average Values for Major Vibrational Frequencies for Aquo Ions (cm^{-1}) for the 32-Water Molecule Clusters[a] (Standard Deviations in Parentheses)

bicarbonate	B3LYP	PBE	expt[55,56]
C−OH stretch	1061 (10)	1018 (14)	1017
O=C=O symm stretch/ C−O−H bend	1395 (30)	1360 (30)	1302
O=C=O symm stretch/ C−O−H bend	1455 (20)	1440 (34)	1360
O=C=O asymm stre	1665 (14)	1613 (24)	1630
carbonate	**B3LYP**	**PBE**	**expt[55,56]**
C=O asymm stretch	1432 (14)	1397(30)	1380
C=O asymm stretch	1518 (22)	1467(27)	1436

[a] O=C=O bends near 680 cm^{-1} and C out-of-plane bend near 800 cm^{-1} are diffusely distributed and not indicated.

The average frequencies and standard deviations for the modes (computed from at least 13 sample configurations for each species) contributing most to the isotope fractionation are given in Table 7 for the large systems at the PBE/6-31G* and B3LYP/6-31G* level. In Figure 5 we show the vibrational modes contributing greater than 0.1 (red) and 0.01 (blue) to the RPFR for both the solvated bicarbonate and carbonate ions. The bare dianion CO_3^{2-} has D_{3h} symmetry with a degenerate asymmetric stretching mode (e′ symmetry) and a completely symmetric stretching mode (a_1′ symmetry). The harmonic symmetric stretch in the bare ion cannot contribute to the IFF, as the C atom does not move. The main contributor to the isotope fractionation in the isolated ion is the asymmetric stretch followed by the inversion mode. In our supermolecule model of the solution, the asymmetric modes split and are, as expected, the main modes responsible for the isotopic fractionation. In isolated HCO_3^-, the predominant modes contributing to the isotope fractionation are the C−O stretching modes for the CO_2^- group, the C−O(H) stretch mode and the C−O−H bend. The bend and the high-energy C−O stretch are strongly coupled. The inversion mode also has a significant change on isotopic substitution. These contributions remain the most important ones in solution. The mode with the large-amplitude C−O motion *trans* to the C−O−H bend has a lower frequency than the mode having the C−O motion *cis* to the C−O−H bend. From the standard deviations given in Table 7, and from Figure 5, it is evident that a number of modes from the supermolecules contribute to the fractionation, including solvent modes coupling to the ion modes. This indicates a significant dependence of the vibrational frequencies on the solute−solvent conformation.

Vibrational frequencies for CO_3^{2-}(aq) and HCO_3^-(aq) have been measured;[55,56] however, these are anharmonic frequencies and can only be indirectly[57] compared with the calculated harmonic frequencies used to predict the isotope fractionation factors. For example, the harmonic PBE frequencies are closer to the experimentally measured (anharmonic) frequencies than B3LYP. As indicated in the gas-phase calculations reported above, this closer agreement is not because PBE necessarily does a better job of predicting vibrational frequencies but is because harmonic calculated frequencies are being compared to anharmonic experimental frequencies. Note that for the bicarbonate asymmetric stretch, the average PBE harmonic frequency (1613 cm^{-1}) is *lower* than the experimental anharmonic value, indicating that PBE is underestimating vibrational frequencies in solution, just as it does in the gas-phase calculations in Table 2. The frequencies of CO_2 in aqueous

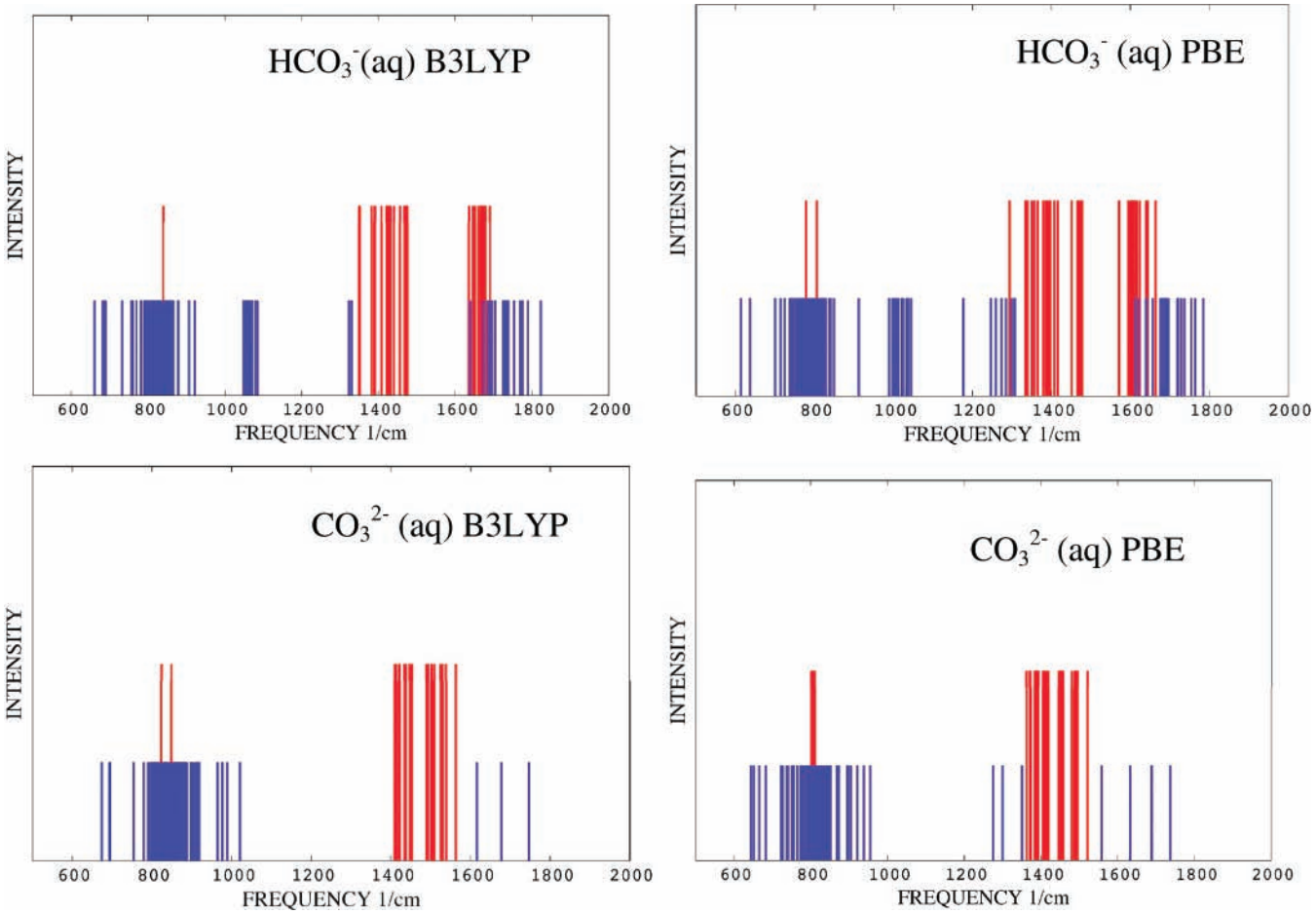

Figure 5. Modes making contributions to the fractionation factor at the 0.1 (red) and 0.01 (blue) levels, for $HCO_3(H_2O)_{32}^-$ (above), and $CO_3(H_2O)_{32}^{2-}$ (below). The graphs on the left are calculated using the B3LYP functional and those on the right are calculated using the PBE functional.

solution have also been measured.[55,58] The assignments between these two papers are inconsistent and the 1995 paper is not consistent with our results for the symmetric stretch.

It is instructive to look in more detail at the contributions to the RPFRs as a function of frequency. These are depicted in Figure 6, which shows the cumulative value of $\beta(\omega)$ for each species. Solvent coupling "rounds off" the steps present at the fractionating frequencies. The coupling is strongest for the librational modes below 1100 cm^{-1} and the H−O−H bending modes 1600−1700 cm^{-1}. Contributions from the O−H stretching band in the 3000−3500 cm^{-1} range are small because the C atom does not move much, if any, in these modes. In the case of CO_2(aq), the solvent coupling is negligible in the DFT approximation. The particular positions of the contributing modes depend on the conformation of the solvent and solute, but the overall conformational dependence of the final RPFR is surprisingly small given the sensitivity of the RPFR to the vibrational frequencies.

III.C. Carbonate Minerals. The frequencies and isotopic shifts of the main fractionating modes calculated using PBE/6-31G*/3-21G are given in Table 8. The RPFRs and IFFs are given in Tables 9 and 10, respectively. The predicted fractionation factors are in reasonably good agreement with experiment,[9,10] and with previous calculations using a more rigorous lattice dynamics approach.[15] One would expect that the Γ-point frequencies reported in ref 15 would be closer to our calculations (which do not include the phonon contribution), and this is indeed the case. However, one must keep in mind that the exchange−correlation function/basis set error cancellation persists in the solid state, at least in the case of calcite; a very high RPFR value (1.2107) is obtained for calcite with B3LYP/6-31G*/3-21G. Using the aug-cc-pVDZ basis on the central carbonate reduces the RPFR to 1.2073. It is difficult to know how to compare the plane-wave basis sets of ref 15 with the Gaussian basis sets used here.

IV. Discussion

We have further tested and improved the supermolecule approach for the ab initio prediction of isotope fractionation by including information from systematically collected multiple configurations. Our calculations based on solvent configuration sampling suggest that with approximately 10 configurations, the standard error in the mean is close to 0.5 per mil and is less important than the computational method/model (e.g., the choice of basis set, the size of the solvation shell chosen to represent the system, and for DFT, the choice of exchange−correlation functional). This finding is an argument in favor of using the static supermolecule approach[12,38] rather than a molecular dynamics approach[14] to predict isotopic fractionation. The benefit of including very large numbers of configurations (i.e., more than 10−20) through thermal averaging using a dynamics-based method does not appear to be an important factor in predicting isotopic fractionation (although there might be other arguments in favor of the dynamics approach, for example, including anharmonic frequency softening). Despite the rather wide variation in the particular positions of the major fractionating modes, there appears to be a compensation effect, making the net predicted RPFR relatively insensitive to these variations. This is similar to what is found for predictions of the free energy

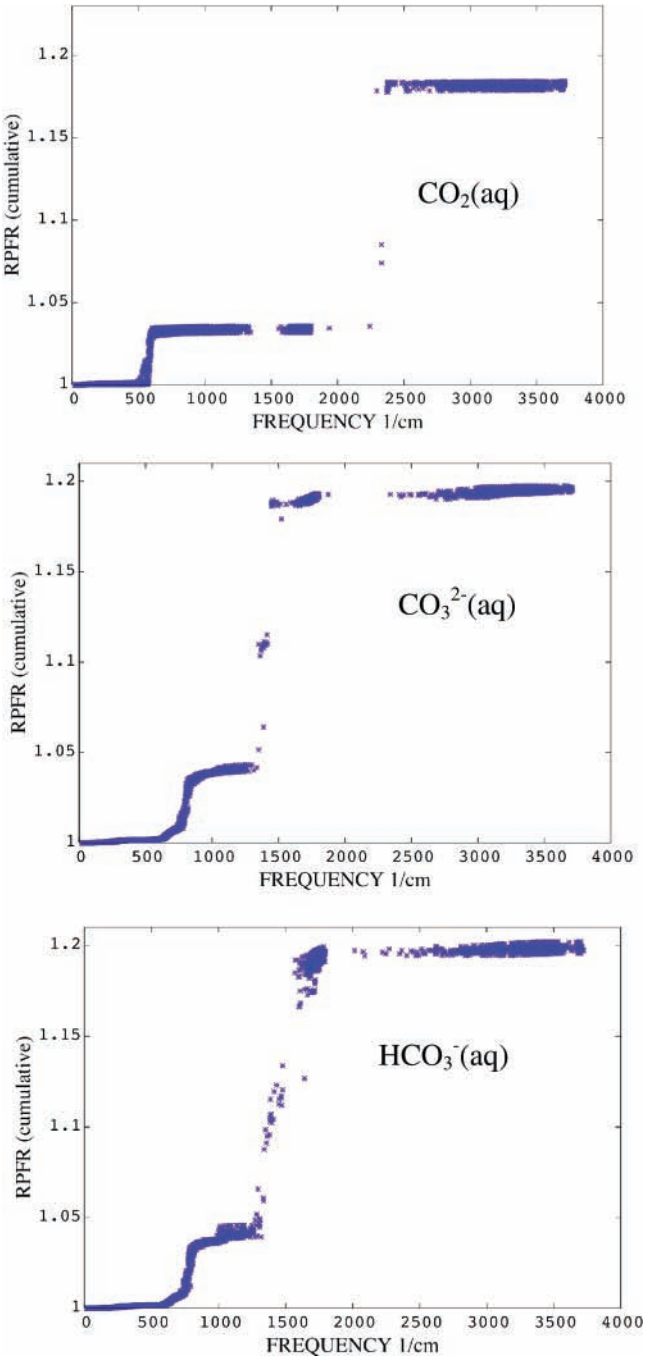

Figure 6. Cumulative contribution to the reduced partition function ratio (β) for $CO_2(H_2O)_{32}$ (top), $CO_3(H_2O)_{32}^{2-}$ (middle), and $HCO_3(H_2O)_{32}^{-}$ (bottom) for all conformations calculated using PBE/6-31G*.

of solvation of ions where a single, dominant configuration provides a very good estimate of this property.[59−61] On the other hand, the results shown in Table 6 indicate that it is important to consider more than a single solvent−solute conformer when calculating isotope fractionation factors in aqueous systems to ensure that one does not have an unrepresentative conformer.

Calculations on the smaller clusters with the larger basis set with diffuse functions give some insight into why the PBE/6-31G* combination appears to work well. In predicting the RPFR, the small-cluster results show that changing the exchange−correlation functional from B3LYP to PBE (hybrid to pure exchange−correlation functional) has an effect similar to improving the basis set from 6-31G* to aug-cc-pVDZ. The PBE/6-31G* combination is thus similar to the B3LYP/aug-cc-pVDZ combination. The reason that the PBE/6-31G* combination is closer to experiment than B3LYP/6-31G* for the larger clusters is because one has a cancellation of errors between the use of a smaller basis set and the use of a pure DFT exchange−correlation functional. The agreement between the estimated and calculated RPFRs for single conformations of the large systems at the B3LYP/aug-cc-pVDZ supports this observation. Thus, the B3LYP/aug-cc-pVDZ combination is probably the most accurate, consistent with previous results showing that hybrid functionals and diffuse basis functions improve the description of hydrogen bonding in aqueous systems.[62−64] However, the aug-cc-pVDZ basis is much more expensive computationally than the 6-31G* basis (1404 vs 632 basis functions for the 32-water systems with CO_3^{2-}) and the pure PBE functional has a better formal scaling of N^3 versus N^4 for B3LYP for N basis functions.

The results in Figure 4 for the temperature dependence of the fractionation between the aqueous species and CO_2(g) show that whereas the PBE/6-31G* calculations are successful in reproducing relative equilibrium fractionation factors of all major

TABLE 8: Cluster Model Calculations of Frequencis (cm^{-1}) for Mineral Systems[a]

mineral	ν_1	ν_2	ν_3	ν_{3b}	ν_4	ν_{4b}	source
calcite	1078	823	1478	1478	685	684	^{12}C
	1078	798	1436	1436	683	682	^{13}C
calcite[b]	1101	868	1497	1497	708	708	^{12}C
	1101	842	1455	1455	706	706	^{13}C
	1083	875	1433	1434	713	713	expt
dolomite	1092	830	1498	1498	702	701	^{12}C
	1092	806	1456	1456	700	699	^{13}C
	1092	881	1441	1441	724	724	expt
magnesite	1099	833	1519	1519	720	720	^{12}C
	1099	810	1477	1477	718	718	^{13}C
	1098	885	1465	1465	753	753	expt
aragonite	1076	835	1503	1474	683	677	^{12}C
	1076	810	1461	1433	681	675	^{13}C
	1084	862	1481	1472	712	700	expt

[a] ν_1: CO_3 symmetric stretch. ν_2: CO_3 inversion. ν_3: C−O asymmetric stretch. ν_4: O−C−O bend. Experimental values (anharmonic) are taken from the compilation in ref 68. [b] Calculation done with the B3LYP functional and the aug-cc-pVDZ basis on the central carbonate.

TABLE 9: Cluster Model Calculations of RFPRS for Mineral Systems[a]

β	25 °C	100 °C	300 °C
calcite	1.1994 (1.2107[b])	1.1390	1.0666
ref 51	1.2037		
ref 68	1.1973		
ref 15	1.2043	1.4215	1.0679
aragonite	1.2014		
ref 15	1.2067		
dolomite	1.2032	1.1417	1.0681
ref 15	1.2072	1.1442	1.0703
magnesite	1.2074		
ref 15	1.2073		

[a] Calculations, unless otherwise indicated, are at the PBE/6-31G*/3-21G level. [b] Calculation done at B3LYP/6-31G*/3-21G.

TABLE 10: Cluster Model Calculations of Isotope Fractionation Factors (per Mil) for Mineral Systems

IFF	calc	expt	lattice dynamics[a]
$\epsilon_{\text{calcite−bicarbonate}}$	0.4	0.9	
$\epsilon_{\text{calcite−CO2(g)}}$	11.5	9.0	
$\epsilon_{\text{aragonite−calcite}}$	1.7	1.8	2.0
$\epsilon_{\text{magnesite−calcite}}$	6.7		5.3
$\epsilon_{\text{dolomite−calcite}}$ (100 °C)	2.4	1.5	1.8
$\epsilon_{\text{dolomite−calcite}}$ (300 °C)	1.4	0.7	1.0

[a] Calculations listed under "lattice dynamics" heading are taken from ref 15.

inorganic carbon reservoirs, improvements are still needed before truly quantitative ~1 per mil (or less) accuracy can be approached. Calculations on the $CO_3{\cdot}32H_2O^{2-}$ and $HCO_3{\cdot}32H_2O^{-}$ single conformers at the B3LYP/aug-cc-pVDZ level are close to this level of accuracy, and the level of agreement between the extrapolated results of the multiconformer systems at the B3LYP/6-31G* level, especially for bicarbonate (which is known with higher accuracy) is encouraging. As mentioned in the Introduction, experimental scatter in the ϵ values reported between different laboratories has been close to 3 per mil, especially for the CO_3^{2-}/CO_2(g) fractionation.[7] However, reports of significantly higher HCO_3^{-}/CO_2(g) fractionations have largely been discounted[6] and it seems unlikely that the experimental results of Zhang et al.[4] are in error by more than 0.5 per mil, even for carbonate.

Several avenues could be explored to improve our calculations. In terms of isotopic fractionation, we have not looked at the issue of size convergence beyond 32 water molecules. The DFT-MD calculations on the 64-water systems suggests that it would be of interest to check the calculations on the aqueous species with even more water molecules at the same level of theory; it appears that approximately 64 waters may be necessary to fully define the second solvation shell. Such explorations could also include the presence of counterions such as Na^+ either as a tight ion pair or as a separate solvated ion in the large supermolecule cluster, although this would probably require more than 64 water molecules. Previous studies on smaller systems show some indication that ion pairs may be important in determining fractionation factors.[8] However, it has not yet been shown if counterions are important if there are a large number of solvent molecules beyond the first solvation shell. The results presented here imply that counterions are probably not needed for 1 per mil accuracy. Another task is to improve the electronic structure treatment such as by using molecular orbital theory with a treatment of correlation at the MP2 level with a basis set including diffuse functions such as the augmented correlation-consistent basis sets aug-cc-pVDZ or aug-cc-pVTZ on the large 32 water clusters studied here at the DFT level with the PBE and B3LYP functionals. Although calculations on the small systems indicate that IFFs obtained with MP2/aug-cc-pVDZ are very close to B3LYP/aug-cc-pVDZ for the ionic species, MP2 calculations include some of the correlation effects needed to treat weak interactions such as the ones under investigation here and would be especially important in the treatment of the IFF for CO_2(aq) supermolecules. As noted above, current DFT functionals do not include features for the correct prediction of van der Waals forces. MP2 calculations on systems of this size are at the limit of current computational capabilities.[65,66] Another direction would involve incorporating anharmonic corrections, for example, by using vibrational self-consistent field methods.[67]

In terms of the carbonate minerals, we note that a complete analysis of isotopic fractionation in solid-state systems requires a thorough treatment of lattice dynamics.[15,51,68] As indicated in Table 4, our cluster approach yields carbon-isotope fractionations in reasonably good agreement with experiment and with other calculations. However, the contribution from the phonons (i.e., beyond the Γ-point) is missing and this is manifested in the better agreement of our results with the Γ-point fractionation factors reported in ref 15. The Pauling bond strength-conserving termination method implemented here places calculations on the mineral systems on the same footing as calculations on the aqueous and gas-phase systems and allows an easily implemented pathway to explicitly correlated molecular orbital-based approaches discussed above, such as MP2 and coupled-cluster theory with augmented correlation-consistent basis sets to mineral systems with currently available software. Such calculations would provide a useful complement to the more traditional lattice dynamics approach, that is restricted, in general, to DFT and HF calculations that can be of limited accuracy due to the pseudopotential approximation in the case of plane-wave basis sets, or with convergence difficulties associated with diffuse basis functions, in the case of periodic codes with Gaussian basis sets.

An interesting result is the breadth of the distribution of vibrational frequencies that contribute to the isotope fractionation factor in the supermolecule approach. For the bare ions, CO_3^{2-} has 6 vibrational modes and HCO_3^{-} has 9 vibrational modes. Figure 5 shows that substantially more modes are involved in the prediction of the IFF. We note especially that there is a strong coupling of the high-frequency C−O stretches with the H_2O bends in the solvent. In addition, there is a coupling of the HOC bend with the solvent bends in the case of HCO_3^{-}. We also note that at frequencies below 1000 cm^{-1} there is little coupling of the low-frequency C−O stretch or of the inversion mode with the solvent modes in terms of a large contribution to the IFF. However, there can be smaller mixings of these modes with the solvent modes in this lower frequency region. Our results show that the local solvent environment can play a role in determining IFFs. This implies that IFFs could be quite different in the different microenvironments present in geological systems, for example, in interfacial environments.

Another practical implication of this work for the carbonate system in particular is that we now have a solid foundation for calculations of other aqueous−carbonate systems where experimental measurements are difficult. For example, the isotopic composition of trace carbonate components in minerals formed in paleo-soils is important for the calculation of atmospheric CO_2 levels in the geologic past.[69] Establishing that these fractionation factors can be calculated accurately will increase the usefulness of computational chemistry in unraveling the molecular-level details of paleoclimate reconstruction, helping to answer questions concerning the precise timing of the recording of isotopic signatures during aqueous-mediated crystal growth processes associated with mineral formation in geological environments.[70]

V. Conclusions

The calculations presented here point to the following conclusions. First, in large clusters with around 30 water molecules forming two solvent shells, conformational variability associated with about 10 configurations gives standard errors in the reduced partition function ratios of approximately 0.5 per mil, which is small compared to nonsystematic errors resulting from the choice of computational method. Second, solvated clusters involving around 30 water molecules, without additional treatment of solvation effects, and with frequencies calculated at the PBE/6-31G* level, are capable of giving qualitative calculation of isotopic fractionation in the gas-phase, aqueous, and solid-state carbonate system with errors $\leq$3 per mil. Part of this success results from a cancellation of errors associated with using a combination of the small basis set, which tends to overestimate the reduced partition function ratios, with the PBE exchange−correlation functional, which tends to underestimate them. Calculations presented here indicate that this error could be reduced to approximately 1 per mil at the B3LYP/aug-cc-pVDZ level. The calculated temperature dependence of the fractionation factors agrees well with experimental

measurements. Calculations with smaller numbers of water molecules cannot achieve this level of accuracy, and calculations using only continuum solvent are not even qualitatively correct, regardless of the type of solvation model employed. Third, calculations on cluster models of carbonate minerals, using the same computational methods as used in modeling the aqueous systems, give good estimates of carbon-isotope fractionations for mineral−aqueous−gas systems. Thus, quantum-chemical approaches allow a comprehensive theoretical integration of the relative isotopic fractionation factors for the gas, aqueous, and mineral phases of importance in the Earth's carbon cycle. Fourth, there is a mixing of the modes of the ion with the solvent leading to more than the minimal number of vibrational modes in the ion being important in determining the isotope fractionation factor.

Acknowledgment. We acknowledge illuminating discussions with J. A. Tossell of the University of Maryland, S. S. Xantheas of Pacific Northwest National Lab, and E. A. Schauble of UCLA. We are grateful to Dr. Eric J. Bylaska of Pacific Northwest National Lab for help with the Car−Parrinello molecular dynamics simulations. Comments from two anonymous reviewers improved the manuscript. We are particularly grateful to one of them who suggested that the Redlich−Teller product rule be checked for the continuum solvent calculations. This work was supported by a grant from the U.S. DOE DE-FG02-04ER15498 to J.R.R. and D.A.D. D.A.D. also thanks the Robert Ramsay Chair Fund of The University of Alabama for support. We thank the Molecular Science Computing Facility of the Environmental Molecular Science Laboratory, a U.S. DOE user facility, for a generous grant of computer time.

Supporting Information Available: Tables of bond lengths (Table S1) and vibrational frequencies (Table S2) for the ionic species in the gas phase and SCRF with no explicit water molecules. This material is available free of charge via the Internet at http://pubs.acs.org.

References and Notes

(1) Thode, H. G.; Shima, M.; Rees, C. E.; Krishnam, K. V. *Can. J. Chem.* **1965**, *43*, 582.
(2) Deuser, W. G.; Degens, E. T. *Nature* **1967**, *215*, 1033.
(3) Lesniak, P. M.; Sakai, H. *Earth Planet. Sci. Lett.* **1989**, *95*, 297.
(4) Zhang, J.; Quay, P. D.; Wilbur, D. O. *Geochim. Cosmochim. Acta* **1995**, *59*, 107.
(5) Halas, S.; Szaran, J.; Niezgoda, H. *Geochim. Cosmochim. Acta* **1997**, *61*, 2691.
(6) Lesniak, P. M.; Zawidzki, P. *Chem. Geol.* **2006**, *231*, 203.
(7) Zeebe, R. E.; Wolf-Gladrow, D. *CO_2 Seawater: Equilibrium, Kinetics, Isotopes*; Halpern, D., Ed.; Elsevier Oceanography Series; Elsevier: Amsterdam, 2001; Vol. 65.
(8) Tossell, J. A. *Inorg. Chem.* **2006**, *45*, 5961.
(9) Rubinson, M.; Clayton, R. N. *Geochim. Cosmochim. Acta* **1969**, *33*, 997.
(10) Romanek, C. S.; Grossman, E. L.; Morse, J. W. *Geochim. Cosmochim. Acta* **1992**, *56*, 419.
(11) Zeebe, R. E. *Geochim. Cosmochim. Acta* **2005**, *69*, 2753.
(12) Liu, Y.; Tossell, J. A. *Geochim. Cosmochim. Acta* **2005**, *69*, 3995.
(13) Klochko, K.; Kaufman, A. J.; Yao, W. S.; Byrne, R. H.; Tossell, J. A. *Earth Planet. Sci. Lett.* **2006**, *248*, 276.
(14) Rustad, J. R.; Bylaska, E. J. *J. Am. Chem. Soc.* **2007**, *129*, 2222.
(15) Schauble, E. A.; Ghosh, P.; Eiler, J. M. *Geochim. Cosmochim. Acta* **2006**, *70*, 2510.
(16) Weil, D. A.; Dixon, D. A. *J. Am. Chem. Soc.* **1985**, *107*, 6859.
(17) Dong, H.; Liu, W.; Doren, D.; Wood, R. *J. Phys. Chem. B* **2006**, *110*, 18504.
(18) Stillinger, F. H.; Weber, T. A. *J. Phys. Chem.* **1983**, *87*, 2833.
(19) Parr, R. G.; Yang, W. *Density Functional Theory of Atoms and Molecules*; Oxford University Press: New York, 1989. Labanowski, J., Andzelm, J., Eds. *Density Functional Methods in Chemistry*; Springer-Verlag: New York, 1991.
(20) Møller, C.; Plesset, M. S. *Phys. Rev.* **1934**, *46*, 618.
(21) Pople, J. A.; Binkley, J. S.; Seeger, R. *Int. J. Quantum Chem. Symp.* **1976**, *10*, 1.
(22) Urey, H. C. *J. Chem. Soc.* **1947**, *562*.
(23) Bigeleisen, J.; Mayer, M. G. *J. Chem. Phys.* **1947**, *15*, 261.
(24) Redlich, O. *Z. Phys. Chem. B* **1935**, *28*, 371. The work of E. Teller (unpublished) is quoted by: Angus, W. R.; Bailey, C. R.; Hale, J. B.; Ingold, C. K.; Leckie, A. H.; Raisin, C. G.; Thompson, J. W.; Wilson, C. W. *J. Chem. Soc.* **1936**, 971. Herzberg, G. *Molecular Spectra and Molecular Structure II. Infrared and Raman Spectra of Polyatomic Molecules*; Van Nostrand: New York, 1945; pp 231−238.
(25) Tomasi, J.; Mennucci, B.; Cammi, R. *Chem. Rev.* **2005**, *105*, 2999.
(26) Frisch, M. J.; Trucks, G. W.; Schlegel, H. B.; Scuseria, G. E.; Robb, M. A.; Cheeseman, J. R.; Montgomery, J. A., Jr.; Vreven, T.; Kudin, K. N.; Burant, J. C.; Millam, J. M.; Iyengar, S. S.; Tomasi, J.; Barone, V.; Mennucci, B.; Cossi, M.; Scalmani, G.; Rega, N.; Petersson, G. A.; Nakatsuji, H.; Hada, M.; Ehara, M.; Toyota, K.; Fukuda, R.; Hasegawa, J.; Ishida, M.; Nakajima, T.; Honda, Y.; Kitao, O.; Nakai, H.; Klene, M.; Li, X.; Knox, J. E.; Hratchian, H. P.; Cross, J. B.; Bakken, V.; Adamo, C.; Jaramillo, J.; Gomperts, R.; Stratmann, R. E.; Yazyev, O.; Austin, A. J.; Cammi, R.; Pomelli, C.; Ochterski, J. W.; Ayala, P. Y.; Morokuma, K.; Voth, G. A.; Salvador, P.; Dannenberg, J. J.; Zakrzewski, V. G.; Dapprich, S.; Daniels, A. D.; Strain, M. C.; Farkas, O.; Malick, D. K.; Rabuck, A. D.; Raghavachari, K.; Foresman, J. B.; Ortiz, J. V.; Cui, Q.; Baboul, A. G.; Clifford, S.; Cioslowski, J.; Stefanov, B. B.; Liu, G.; Liashenko, A.; Piskorz, P.; Komaromi, I.; Martin, R. L.; Fox, D. J.; Keith, T.; Al-Laham, M. A.; Peng, C. Y.; Nanayakkara, A.; Challacombe, M.; Gill, P. M. W.; Johnson, B.; Chen, W.; Wong, M. W.; Gonzalez, C.; Pople, J. A.; *Gaussian 03*, revision C.02; Gaussian, Inc.: Wallingford, CT, 2004.
(27) Perdew, J. P.; Burke, K.; Ernzerhof, M. *Phys. Rev. Lett.* **1996**, *77*, 3865.
(28) Perdew, J. P.; Wang, Y. *Phys. Rev. B* **1991**, *45*, 13244.
(29) Burke K.; Perdew J. P.; Wang, Y. In *Electronic Density Functional Theory: Recent Progress and New Directions*; Dobson, J. F., Vignale, G., Das, M. P., Eds.; Plenum: New York, 1997; pp 81−122.
(30) Becke, A. D. *Phys. Rev. A* **1988**, *38*, 3098.
(31) Perdew, J. P. *Phys. Rev. B* **1986**, *33*, 8822.
(32) Becke, A. D. *J. Chem. Phys.* **1993**, *98*, 5648.
(33) Lee, C.; Yang, W.; Parr, R. G. *Phys. Rev. B* **1998**, *37*, 785.
(34) Kendall, R. A.; Dunning, T. H., Jr.; Harrison, R. J. *J. Chem. Phys.* **1992**, *96*, 6796.
(35) Tomasi, J.; Cammi, R.; Mennucci, B. *Int. J. Quantum Chem.* **1999**, *75*, 783.
(36) Klamt, A.; Schuurmann, G. *J. Chem. Soc., Perkin Trans.* **1993**, *2*, 799.
(37) Parallel Quantum Solutions, http://www.pqs-chem.com.
(38) Oi, T.; Yanase S. *J. Nucl. Sci. Technol.* **2001**, *38*, 429.
(39) Baker, J.; Pulay, P. *J. Comput. Chem.* **2000**, *21*, 69.
(40) Car, R.; Parrinello, M. *Phys. Rev. Lett.* **1985**, *55*, 2471.
(41) Bylaska, E. J.; de Jong, W. A.; Kowalski, K.; Straatsma, T. P.; Valiev, M.; Wang, D.; Aprà, E.; Windus, T. L.; Hirata, S.; Hackler, M. T.; Zhao, Y.; Fan, P.-D.; Harrison, R. J.; Dupuis, M.; Smith, D. M. A.; Nieplocha, J.; Tipparaju, V.; Krishnan, M.; Auer, A. A.; Nooijen, M.; Brown, E.; Cisneros, G.; Fann, G. I.; Früchtl, H.; Garza, J.; Hirao, K.; Kendall, R.; Nichols, J. A.; Tsemekhman, K.; Wolinski, K.; Anchell, J.; Bernholdt, D.; Borowski, P.; Clark, T.; Clerc, D.; Dachsel, H.; Deegan, M.; Dyall, K.; Elwood, D.; Glendening, E.; Gutowski, M.; Hess, A.; Jaffe, J.; Johnson, B.; Ju, J.; Kobayashi, R.; Kutteh, R.; Lin, Z.; Littlefield, R.; Long, X.; Meng, B.; Nakajima, T.; Niu, S.; Pollack, L.; Rosing, M.; Sandrone, G.; Stave, M.; Taylor, H.; Thomas, G.; van Lenthe, J.; Wong, A.; Zhang, Z. *NWChem, A Computational Chemistry Package for Parallel Computers*, version 4.7; Pacific Northwest National Laboratory: Richland, WA 99352−0999; 2006.
(42) Kendall, R. A.; Aprà, E.; Bernholdt, D. E.; Bylaska, E. J.; Dupuis, M.; Fann, G. I.; Harrison, R. J.; Ju, J.; Nichols, J. A.; Nieplocha, J.; Straatsma, T. P.; Windus, T. L.; Wong, A. T. *Comput. Phys. Commun.* **2000**, *128*, 260.
(43) Troullier, N.; Martins, J. L. *Phys. Rev. B* **1991**, *43*, 1993.
(44) Bloechl, P. E.; Parrinello, M. *Phys. Rev. B* **1992**, *45*, 9413.
(45) Baker, J. *J. Comput. Chem.* **1986**, *7*, 385.
(46) Baker, J.; Fusti-Molnar, L.; Pulay, P. *J. Phys. Chem. A* **2004**, *108*, 3040.
(47) de Villiers, J. P. R. *Am. Mineral.* **197**1, *56*, 758.
(48) Graf, D. L. *Am. Mineral.* **1961**, *46*, 1283.
(49) Althoff, P. L. *Am. Mineral.* **1977**, *62*, 772.
(50) Head, J. D. *Int. J. Quantum Chem.***199**7, *65*, 827.
(51) Chacko, T.; Mayeda, T. K.; Clayton, R. N.; Goldsmith, J. R. *Geochim. Cosmochim. Acta* **1991**, *55*, 2867.
(52) Herzberg, G. *Molecular Spectra and Molecular Structure. III. Electronic Spectra and Electronic Structure of Polyatomic Molecules*; Van Nostrand Reinhold: New York, 1966; p 598.
(53) Tashkun, S. A.; Perevalov, V. I.; Teffo, J.-L.; Rothman, L. S.; Tyuterev, V. G. *J. Quantum Spectrosc. Radiat. Transfer* **1998**, *60*, 785.

(54) Ding, Y.; Macko, P.; Romanini, D.; Perevalov, V. G.; Tashkun, S. A.; Teffo, J.-L.; Hu, S.-M.; Campargue, A. *J. Mol. Spectrosc.* **2004**, *226*, 146.

(55) Davis, A. R.; Oliver, B. G. *J. Solution Chem.* **1972**, *1*, 329.

(56) Rudolph, W. W.; Fischer, D.; Irmer, G. *Appl. Spectrosc.* **2006**, *60*, 130.

(57) Xantheas, S. S. *Int. Rev. Phys. Chem.* **2006**, *25*, 719.

(58) Berger, A. J.; Wang, Y.; Sammeth, D. M.; Itzkan, I.; Kneipp, K.; Feld, M. S. *Appl. Spectrosc.* **1995**, *49*, 1164.

(59) Zhan, C.-G.; Dixon, D. A. *J. Phys. Chem. A* **2001**, *105*, 11534. Zhan, C.-G.; Dixon, D. A. *J. Phys. Chem. A* **2002**, *106*, 9737. Zhan, C.-G.; Dixon, D. A. *J. Phys. Chem. A* **2003**, *107*, 4403. Zhan, C.-G.; Dixon, D. A. *J. Phys. Chem. A* **2004**, *108*, 2020.

(60) Tissandier, M. D.; Cowen, K. A.; Feng, W. Y.; Gundlach, E.; Cohen, M. H.; Earhart, A. D.; Tuttle, T. R.; Coe, J. V. *J. Phys. Chem. A* **1998**, *102*, 9308. Tissandier, M. D.; Cowen, K. A.; Feng, W. Y.; Gundlach, E.; Cohen, M. H.; Earhart, A. D.; Coe, J. V.; Tuttle, T. R. *J. Phys. Chem. A* **1998**, *102*, 7787. Tuttle, T. R.; Malaxos, S.; Coe, J. V. *J. Phys. Chem. A* **2002**, *106*, 925. Coe, J. V. *Int. Rev. Phys. Chem.* **2001**, *20*, 33.

(61) Topol, I. A.; Tawa, G. J.; Burt, S. K.; Rashin, A. A. *J. Chem. Phys.* **1999**, *111*, 10998. Tawa, G. J.; Topol, I. A.; Burt, S. K.; Caldwell, R. A.; Rashin, A. A. *J. Chem. Phys.* **1998**, *109*, 4852.

(62) Xantheas, S. S. *J. Chem. Phys.* **1995**, *102*, 4505.

(63) Sim, F.; St. Amant, A.; Papai, I.; Salahub, D. R. *J. Am. Chem. Soc.* **1992**, *114*, 4391.

(64) Hamman, D. R. *Phys. Rev. B* **1997**, *55*, R10157.

(65) Fanourgakis, G. S.; Apra, E.; de Jong, W. A.; Xantheas, S. S. *J. Chem. Phys.* **2005**, *122*, Art. No. 134304.

(66) Lagutschenkov, A.; Fanourgakis, G. S.; Niedner-Schatteburg, G.; Xantheas S. S. *J. Chem. Phys.* **2005**, *122*, Art. No. 194340.

(67) Miller, Y.; Chaban, G. M.; Gerber, R. B. *J. Phys. Chem. A* **2005**, *109*, 6565.

(68) Deines, P. *Geochim. Cosmochim. Acta* **2004**, *68*, 2659.

(69) Yapp, C. J.; Poths, H. *Nature* **1992**, *355*, 342.

(70) LeMarchand, D.; Wasserburg, G. J.; Papanastassiou, D. *Geochim. Cosmochim. Acta* **2004**, *68*, 4665.